ACS APPLIED MATERIALS & INTERFACES

Research Article

www.acsami.org

Preparation and Mechanics of Nanotextures on Adapting a Low Adhesive Surface Using Local Oxidation Nanolithography

Yufei Mo,*[,†,‡] Zhaoxia Lu,[†] Alicia Chau,[‡] and Fuchuan Huang*[,†]

[†]Guangxi Key Laboratory of Petrochemical Resource Processing and Process Intensification Technology, Guangxi University, Nanning 530004, P. R. China

[‡]School of Engineering & Applied Science, The George Washington University, Washington DC, 20052, United States

ABSTRACT: This paper describes an application for atomic force microscopy to the fabrication of nanotextures with various features on a GaAs surface by local oxidation nanolithography (LON). By controlling the geometrical shapes and surface coverage of the nanotexture, the surface adhesion can be adjusted to a low adhesive surface. The influence of environmental conditions, such as relative humidity and temperature on adhesion behavior, was studied. An optic heater was employed to minimize thermal effect on an atomic force microscope (AFM) cantilever and $PbZrTiO_3$ scanner. In our study, AFM is used for both fabrication and characterization. LON allows the fabricated nanotextures to be altered in situ without the need to change masks or repeat the entire fabrication process. Furthermore, the nanoadhesion characterization of nanotextures on a GaAs surface was investigated with a colloidal probe method.

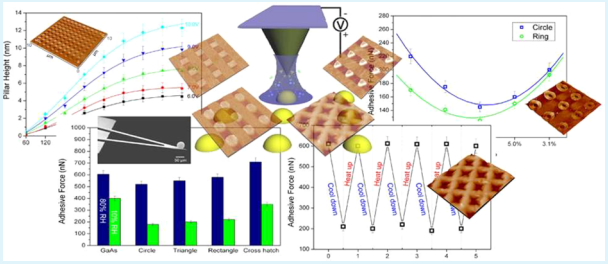

KEYWORDS: *nanotexture, local oxidation nanolithography, adhesion, functional surface*

1. INTRODUCTION

The microelectromechanical system (MEMS) represents an emerging technology that relies on the microfabrication of microscale mechanical components such as mirrors, gears, latches, etc. Those components are integrated with on board actuators. Over the past several decades, MEMS researchers and developers have demonstrated an extremely large number of microsensors for almost every possible sensing modality including temperature, pressure, inertial forces, chemical species, magnetic fields, radiation, etc. However, thus, despite the demonstration of numerous MEMS devices and product concepts each year, a very small number have actually succeeded in the market place. A well-known problem in the fabrication of MEMS devices from surface micromachining is stiction, which occurs when surface adhesion forces are higher than the mechanical restoring force of the microstructure. When a device is removed from the aqueous solution after wet etching the underlying sacrificial layer, the liquid meniscus formed on hydrophilic surfaces pulls the microstructure towards the substrate and stiction occurs; another difficult situation is interface stiction during operation when microstructures come into contact. Interface stiction is caused by capillary forces, electrostatic attraction, and chemical bonding. The difficulty in controlling surface forces is a critical impediment to the fabrication and operation of many MEMS devices.[1−3]

One approach to solve the stiction problem is to provide a low-energy surface thin film in the form of an organic passivation layer on the inorganic surface; for example, a self-assembled monolayer can not only eliminate or reduce capillary forces and direct chemical bonding but also reduce electrostatic forces if the thin organic layer is directly applied to the semiconducting substrate, without the intervening oxide layer. Texas Instruments uses a fluorinated fatty acid self-assembled monolayer (SAM) on the aluminum oxide surface in their digital mirror displayer,[4] while analog devices coat the surfaces of their inertia sensors using thermal evaporation of silicone polymeric materials at the packaging stage after the device is completely released.[5] Another much advocated approach is the formation of siloxane self-assembled monolayers (SAMs) on the oxide terminated surface, but the difficulty of this chemistry and the poor reproducibility put significant limitations on its practical usage.

Another attractive approach to tackle the stiction problem is to fabricate nanotexture on the surface. A surface texture is a predominant layer of machining pattern on the surface. The pattern is a repetitive impression created on the surface of a part. It is often representative of a specific manufacturing operation. The layer may be specified when it has an effect on the function of the part.[6] Compared with SAMs, surface texture can be used on metallic, inorganic, and organic surfaces. Furthermore, surface textures can also be used to reduce adhesion and increase reliability and durability in energy transmission efficiency.

Scanning probe lithography (SPL) is an emerging area of research in which the scanning tunneling microscope (STM) or

Received: February 11, 2013
Accepted: April 30, 2013
Published: April 30, 2013

the atomic force microscope (AFM) is used to pattern nanometer-scale features. Patterning methods include mechanical patterning such as scratching[7−9] or nanoindentation[10,11] or local heating with the sharp tip.[12] Since J. Dagate[13] discovered the probe-based oxidation in the heyday of atomic scale manipulation of surfaces by STM, local oxidation nanolithography has evolved to become a useful tool to fabricate sophisticated nanodevices for studying quantum phenomena such as quantum conductance and coulomb blockade. When a voltage bias is applied between a sharp probe tip and a sample, an intense electric field is generated in the vicinity of the tip. The concentrated field is the enabling element for two other methods, field enhanced oxidation of semiconductor materials or metals and electron exposure of resist materials. Recently, this technology has been used extensively to fabricate nanotextures for an anti-adhesion purpose.

Adhesion at nanoscale is of interest in various scientific disciplines, such as nanocontacts for construction of MEMS in engineering, cell and protein adhesion in microbiology,[14,15] molecular mechanisms in chemistry,[16−18] and microfluidics in physics.[19,20] Adhesive forces come from two sources: contact interfacial forces and noncontact forces such as Van Der Waals or electrostatic forces. Adhesion is typically measured by a pull-off force between the cantilever tip and the surface. The challenge in the measurement often lies when determining the real area of contact. For commercial sharp tips, the surface roughness and high contact pressure may cause the tip to rotate and the surface to deform. W. Ducker[21] introduced the use of colloidal probe tips by attaching a sphere to the cantilever to measure adhesion. The spherical shape of the tip provides controlled contact pressure, symmetry, and mostly elastic contacts. For nanotexture adhesive force measurement, the spherical probe tip can be in full contact with the texture surface, while the sharp tip can only perform point contact.

2. EXPERIMENTAL SECTION AND METHODS

Fabrication of nanotextures was performed by using a commercial AFM (Bruker DI 3100, USA). The local oxidation nanolithography was carried out in noncontact dynamic mode and in the regime of the contact force using silicon cantilevers with electrically conductive tips coated by platinum (Budget Sensor). The tip is conic with a radius below 30 nm. The AFM software is extended with a program package for the well-defined movement of the tip over a sample. The ease of control of other tip−sample parameters makes it possible to accomplish predefined patterns at various pulsed bias voltage, pulsewidth, and write speed in contact mode. For environmental control, relative humidity was controlled by introducing a mixture of dry and moist argon stream inside the booth. The relative humidity was controlled to range from 5% to 85%. The local oxidation nanolithography performed by AFM is illustrated in Figure 1. In this nanolithography process, oxides grow on a chemically reactive substrate by application of a pulse bias voltage between a conductive tip and a sample surface which act as an anode.

Adhesion behavior of the fabricated nanotextures was characterized with an atomic microscope with dynamic force spectroscopy. The influence of relative humidity and temperature on adhesion was studied in a noise and vibration-isolated, environment-controlled booth, as shown in Figure 2a. In order to study the effect of temperature on adhesion, an optic heater was employed to minimize thermal effect on an AFM cantilever and $PbZrTiO_3$ (PZT) scanner while the local region of the sample surface is heating up. A thermocouple and a hygrometer were used to measure the sample relative humidity and temperature, respectively. The temperature ranged from 20 to 160 °C, while the relative humidity ranged from 5% RH to 85%RH during adhesion measurement. To control the contact time independent of the loading rate, a trapezoidal signal from a programmable waveform generator was applied to drive the piezo actuator. In adhesion measurements, the laser beam is focused on the back of the AFM cantilever to detect the cantilever's deflection as it interacts with the surface beneath it. The reflected beam is directed onto a split photodiode detector, which produces a voltage signal proportional to the cantilever deflection. The sample beneath the cantilever is moved using a piezoelectric transducer. In the force measurements, motions in the x and y directions are disabled, the piezoelectric tube is used to move the surface in the z direction, and the cantilever deflection is continuously measured. The surface is first moved toward the cantilever until the tip contacts the surface and then is retracted from the cantilever until the tip snaps off from the surface. The adhesion force was obtained from measuring the deflection of the cantilever at the point where the tip pulls off from the surface after contact. A colloidal probe was prepared by gluing glass beads with radius of 20 μm (SRM1003c, radius range from 10 to 22.5 μm, NIST, MD) onto an individual tipless cantilever. The cantilever used in our experiments was etched from single-crystal silicon, and the force constant of the cantilever was individually calculated using the added mass technique.[22−24] The measured normal force constant of the cantilever was determined to be 0.51 N/m. A typical colloidal probe is shown in Figure 2b. The colloidal probe was cleaned by ethanol and then acetone before use. For all measurements, the same cantilever was used in this comparative study. Furthermore, to avoid influence of molecules which may transfer to the tip on the AFM/FFM experiments, the tip was scanned on a cleaved mica surface to remove these physical adsorbed molecules. The surface topography of the colloidal probe was scanned with a cantilever with force constant of 0.12 N/m and a silicon nitride sharp tip under contact mode. The microroughness of the colloidal probe in root-mean-square was estimated to be 0.3 nm.

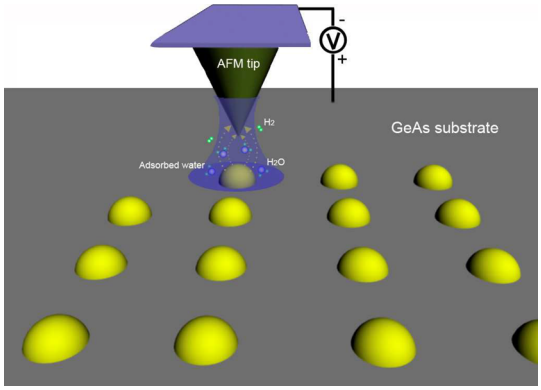

Figure 1. Schematic of the local oxidation nanolithography induced by a conductive AFM tip.

3. RESULTS AND DISCUSSION

3.1. Effect of Pulsed Bias Voltage, Pulsewidth, and Ambient Humidity on GeAs Local Oxidation. Fabrication and application of nanotexture for a study of their quantum properties and for building new nanodevices or surface modifying requires a reliable control of individual technological steps. To be able to prepare nanotexture of specific dimensions and properties, the relationship between the operation parameters should be fully understood. The local oxidation nanolithography is controlled by several major parameters: pulsed bias voltage, pulsewidth, and ambient humidity.

Figure 3 shows a testing array of GaAs oxide pillars prepared at different tip−sample voltages and pulsewidths on GaAs substrate (relative humidity of 50%, temperature of 20 °C). The oxide height is a function of pulsewidth for various tip−sample pulse bias voltages, as shown in the figure. From "b" to "a" in the inset, the pillars were prepared at progressively lower

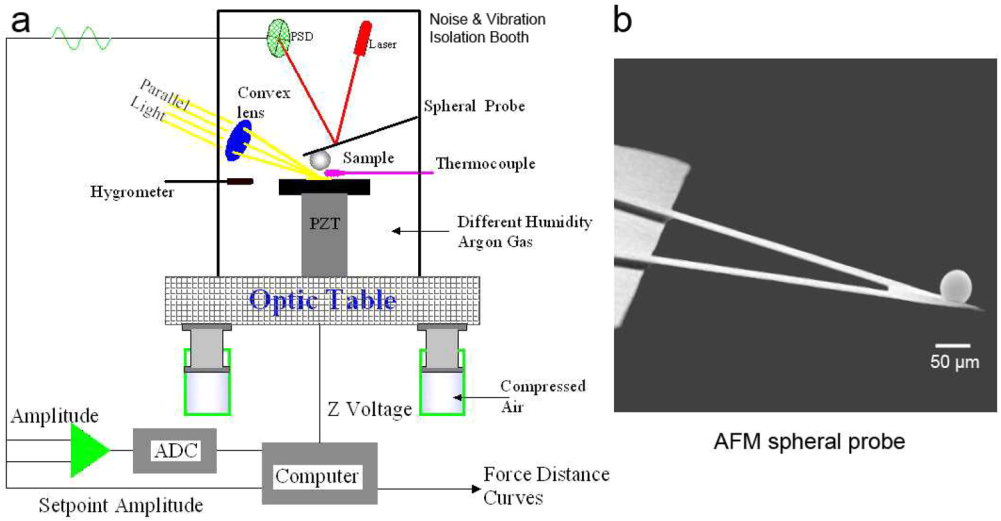

Figure 2. Schematic figure of the AFM system used for adhesion measurement (a); SEM image of the colloidal probe (b).

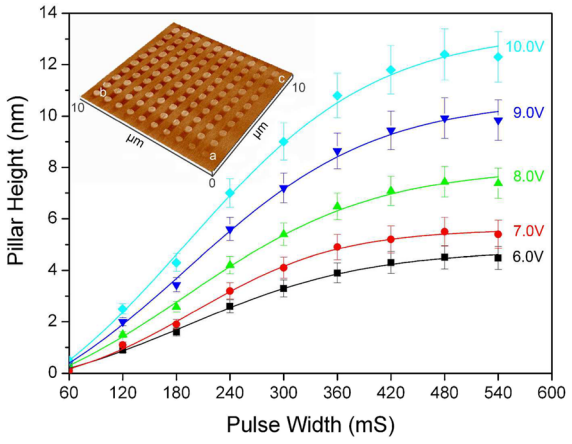

Figure 3. Height growth of GaAs oxide pillars as a function of pulse width for different bias voltages.

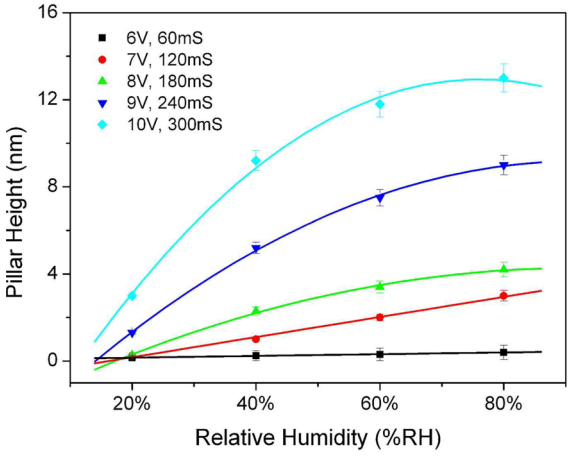

Figure 4. Height growth of GaAs oxide pillars as a function of ambient humidity for different bias voltages and pulse width.

tip−sample pulse bias voltages. On the other hand, going from "c" to "a", the pillars were made at progressively decreasing pulsewidths. Such a testing pillar array makes it possible to find the relations between the height of pattern and operational parameters. In the case of patterning oxide pillars, the effectiveness of the tip−sample pulse bias voltage suggested that the fabrication of pillars can be achieved by varying the pulsewidth. It is evident that the lower pulse bias voltages and short pulsewidths result in lower anodized oxide pillars. The reason for that could be due to insufficient voltage or time for reaching the saturation height. In the anodic oxidation process, the anionic and cationic transports are important factors in determining the kinetics of oxidation. In test conditions, the driving force is the faradic current flowing between the tip and sample surface with the aid of the water meniscus. It is obvious that the pillar was prepared at the highest tip−sample pulse voltage and the longest pulsewidth produce the best developed height. In this experiment, the pillar with the lowest height value (0.3 nm) was treated with a pulse bias voltage of 6.0 V and pulsewidth of 60 ms. On the other hand, the pillar with the highest value (12.3 nm) was achieved at a pulse bias voltage of 10.0 V and pulsewidth of 540 ms.

Figure 4 demonstrates the linear dependences of the oxide height as function of relative humidity. The height of GeAs oxide pillar was proportional to relative humidity for various distinct optional parameters (pulse bias voltage and pulse-width). The reason for that could be due to the different thickness in water film. In any case, the present results demonstrate that the AFM tip-induced local oxidation can be a viable tool for fabricating well-controlled oxide patterns provided proper operation conditions are chosen.

3.2. Geometrical Shape, Temperature, and Humidity Effects of Nanotexture on Adhesion. The local oxidation nanolithography can be used not only in fabrication of nanodevices but also on adhesion−resistance of surface textures. For solid surface contacts without adhesive agents, adhesion is proportional to the real area of contact. As an example of nanotextures, pillars of rectangle, triangle, circle, and crosshatch were fabricated by local oxidation nanolithography for this purpose shown in Figure 5a−d.

Figure 6a shows that adhesive force increased with relative humidity, which is due to water menisci contribution. It is also observed that the adhesive force of textures increased indistinctively and tended to a stable value. Adhesive force of bare GeAs surface is as high as 605/403 nN under humidity of 80%RH/10%RH. Once surface textures of a circle, triangle, and rectangle were fabricated, the adhesive force decreased to 520/

dx.doi.org/10.1021/am401281u | ACS Appl. Mater. Interfaces 2013, 5, 4356−4360

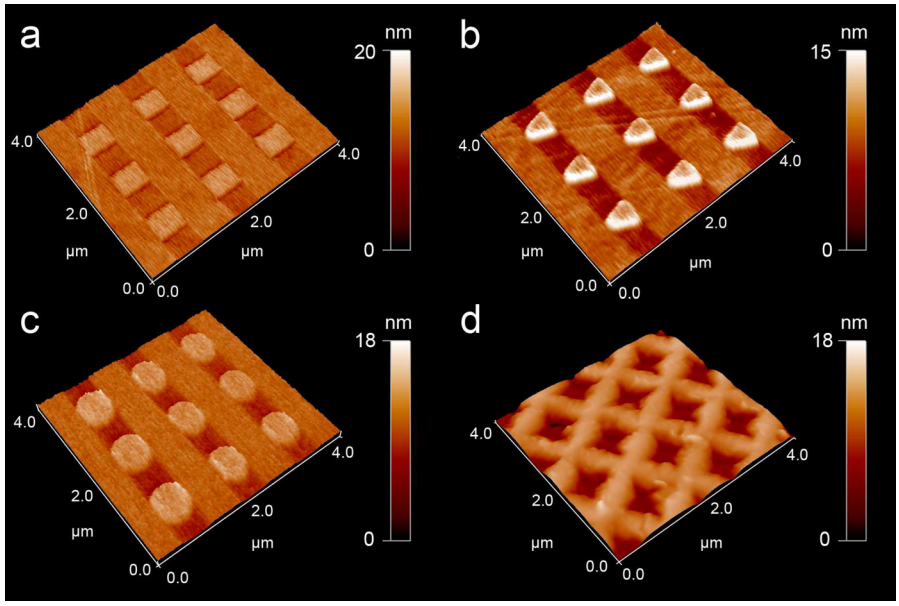

Figure 5. AFM topographies of GeAs oxide nanopillars with various geometrical shapes: rectangle (a), triangle (b), circle (c), and cross hatch (d).

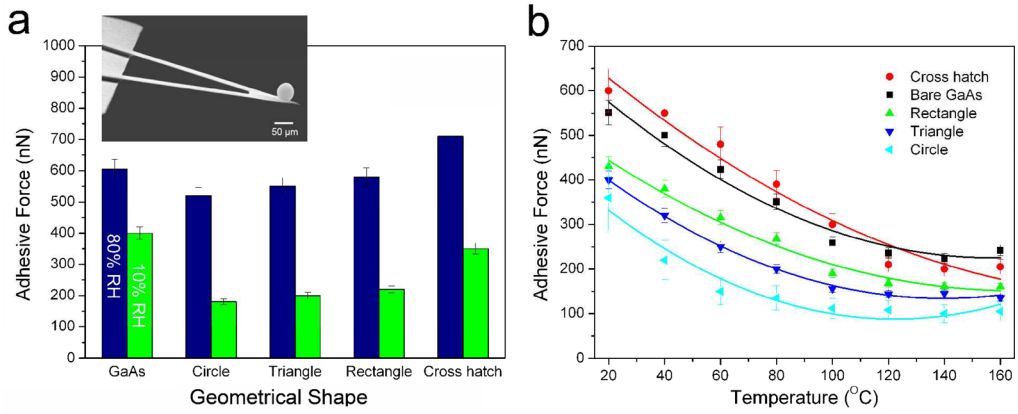

Figure 6. Dependence on relative humidity (a) and temperature (b) of adhesion for GeAs oxide nanopillars.

179, 551/202, and 579/223 nN, respectively. This result indicates that the nanotextures have good adhesion resistance on GeAs surface. Furthermore, the adhesive force was observed to decrease in the following order: cross hatch > rectangle > triangle > circle. However, the cross hatch texture was even higher than the bare GeAs surface under high relative humidity, since the cross hatch structure is more prone to absorb moisture under high relative humidity. Figure 6b shows the influence of temperature (20−160°C) on adhesion. The adhesive force decreased with the increase of temperature and then tended to a stable value. The drop in adhesive force is a result of desorption of water molecules and the corresponding decrease of water menisci contribution. While the temperature is below 100°C, adhesion of cross hatch textured surfaces is higher than that of untextured surfaces. However, the adhesion of the cross hatch textured surface was reduced greatly and was lower than the untextured surface, at temperatures above 120°C. The reason for the adhesion behavior of cross hatch texture may be because evaporation of adsorbed water results in a decreased formation of water menisci than that in the untextured surface. The adhesive force depends primarily on contact interface rather than water menisci contribution under high temperature.

3.3. Hollow Structure and Area Density Effects of Nanotexture on Adhesion. Figure 7 shows adhesive forces for circle and ring nanopillars with surface coverage of 19.6%, 13.6%, 8.7%, 5.0%, and 3.1%. The height of the pillars was kept at about 12 nm; therefore, the nanotextures tend to dominate

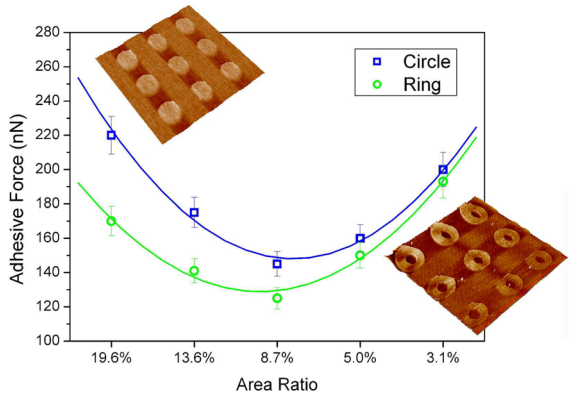

Figure 7. Plots of adhesive forces for circle and ring nanopillars with surface coverage of 19.6%, 13.6%, 8.7%, 5.0%, and 3.1%.

dx.doi.org/10.1021/am401281u | ACS Appl. Mater. Interfaces 2013, 5, 4356−4360

the contact condition when compared to the colloidal probe. It is observed that the adhesive forces are closely related to the surface coverage of nanotextures. The surface coverage relates directly to the bearing ratio, which describes the real area of contact between two solid surfaces.[25] When holding the same nanopillar heights, the higher the surface coverage, the higher is the bearing ratio. Therefore, the adhesive force decreases as the density of nanopillars decreases or as the distance between the nanopillars increase, because low density means fewer contacting points. Larger meniscus area results in higher adhesion. However, the probe tip would contact directly with substrate, and the corresponding adhesive force would increase when the surface ratio is too small to support the contact surface. As surface coverage of the nanopillars increases, not only can each meniscus grow bigger but also the capillary pressure with each meniscus can become higher.[26,27] Both of these changes lead to a higher adhesive force.

3.4. Reversible High to Low Transition of Adhesion. Figure 8 shows a reversible adhesion transition of the cross hatch textured surface. The adhesive force of the cross hatch textured surface changes from high adhesive force to low adhesive force under high temperature. After annealing, the surface was cooled down and placed at room temperature overnight, and a new adhesive force measured the surface adhesion again. The high adhesion surface of the cross hatch texture was obtained. This process was repeated several times, and good reversibility of the surface adhesion was observed.

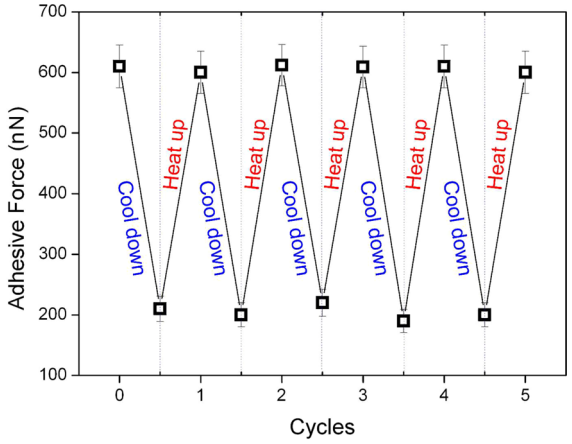

Figure 8. Reversible adhesion transition of the cross hatch textured surface.

4. CONCLUSIONS

In this paper, the application of tip-induced local oxidation nanolithography for fabrication of nanotextures on a GeAs surface is presented. Results indicated that the local oxidation nanolithography is controlled by several major operational parameters such as tip−sample pulse bias voltage, pulsewidth, and relative humidity. The various geometrical shape pillars including rectangle, triangle, circle, and cross hatch were fabricated in height range from 0.3 to 12.3 nm for the purpose of adhesion−resistance. Adhesive force was observed to decrease in the following order: cross hatch > rectangle > triangle > circle. Meanwhile, the adhesive forces showed a close relationship to the surface coverage of nanotextures. The influence of relative humidity and temperature was investigated, and the corresponding adhesive mechanisms were discussed. This technique shall provide a unique opportunity for the exploration of surface force adaptation under spatially well-defined, controlled nanotextures.

AUTHOR INFORMATION

Corresponding Author

*E-mail: yufeimo@gwu.edu (Y.M.); nanolab@gxu.edu.cn (F.H.).

Notes

The authors declare no competing financial interest.

ACKNOWLEDGMENTS

This work was funded by the National Natural Science Foundation of China under Grant No. 51205070 and the Natural Science Foundation of Guangxi under Grant No. 2012GXNSFBA053023.

REFERENCES

(1) Laboriante, I.; Farrokhzad, N.; Fisch, M.; Shavezipur, M.; Carraro, C.; Maboudian, R.; Bai, Q.; Liu, M.; Hoen, S. *J. Micromech. Microeng.* **2012**, *22*, 065031.
(2) De Boer, M. P.; Mayer, T. M. *MRS Bull.* **2001**, *26*, 302−304.
(3) Vincent, M.; Kim, M.; Carraro, C.; Maboudian, R. *Proc. IEEE MEMS Conf.* **2012**, 39−42.
(4) Hornbeck, L. J. U.S. Patent 5602671. February 11, 1997.
(5) Martin, J. R.; Zhao, Y. U.S. Patent 5694740. December 9, 1997.
(6) DeGarmo, E. P.; Black, J. T.; Kohser, R. A. *Materials and Processes in Manufacturing*; Wiley: Hoboken, NJ, 2003; ISBN: 0-471-65653-4.
(7) Bu, D.; Mullen, T. J.; Liu, G. *ACS Nano* **2010**, *4*, 6863−6873.
(8) Garno, J. C.; Yang, Y.; Amro, N. A. *Nano Lett.* **2003**, *3*, 389−395.
(9) Yang, Y. D.; Hu, Z. J.; Zhao, X. S.; Sun, T.; Dong, S.; Li, X. D. *Small* **2010**, *6*, 724−728.
(10) Calabri, L.; Pugno, N.; Menozzi, C.; Valeri, S. *J. Phys.: Condens. Matter.* **2008**, *20*, 474208.
(11) Li, X. D.; Wang, X. N.; Xiong, Q. H.; Eklund, P. C. *Appl. Phys. Lett.* **2005**, *87*, 233113.
(12) Greiner, C.; Felts, J. R.; Dai, Z.; King, W. P.; Carpick, R. W. *Nano Lett.* **2010**, *10*, 4640−4645.
(13) Dagata, J. A. *Science* **1995**, *270*, 1625−1626.
(14) Alsteens, D.; Dupres, V.; Klotz, S. A.; Gaur, N. K.; Lipke, P. N.; Dufrene, Y. F. *ACS Nano* **2009**, *3*, 1677−1682.
(15) Palacio, M.; Schricker, S.; Bhushan, B. *J. Microsc.* **2010**, *240*, 239−248.
(16) Stiernstedt, J.; Nordgren, N.; Wågberg, L.; Brumer, H. Y.; Gray, D. G.; Rutland, M. W. *J. Colloid Interface Sci.* **2006**, *303*, 117−123.
(17) Mo, Y.; Bai, M. *Surf. Interface Anal.* **2009**, *41*, 602−609.
(18) Mo, Y.; Huang, F. *Surf. Interface Anal.* **2012**, *44*, 554−558.
(19) Mohanty, S. *Lab Chip* **2012**, *12*, 3624−3636.
(20) Voyvodic, P. L.; Min, D.; Baker, A. B. *Lab Chip* **2012**, *12*, 3322−3330.
(21) Ducker, W. A.; Senden, T. J.; Pashley, R. M. *Nature* **1991**, *353*, 239−241.
(22) Cleveland, J.; Manne, S. *Rev. Sci. Instrum.* **1993**, *64*, 403−405.
(23) Mo, Y.; Bai, M. *J. Colloid Interface Sci.* **2009**, *333*, 304−309.
(24) Bhushan, B. *Handbook of micro/nano tribology*, 2nd ed.; CRC Press: Boca Raton, FL, 1994.
(25) Teuschler, T.; Mahr, K.; Miyazaki, S.; Hundhausen, M.; Ley, L. *Appl. Phys. Lett.* **1995**, *67*, 3144.
(26) Avouris, P.; Hertel, T.; Martel, R. *Appl. Phys. Lett.* **1997**, *71*, 285.
(27) Cervenka, J.; Kalousek, R.; Bartosik, M.; Skoda, D.; Tomanec, O.; Sikola, T. *Appl. Surf. Sci.* **2006**, *253*, 2373−2378.